Contribution of higher-order processes to the damping of hot giant dipole resonance

Nguyen Dinh Dang,[1,*] Kosai Tanabe,[1] and Akito Arima[2]
[1]*Department of Physics, Saitama University, 255 Shimo-Okubo, Urawa, Saitama 338-8570, Japan*
[2]*RIKEN, Wako, Saitama 351-01, Japan*
(Received 4 June 1998)

A systematic study is presented for three characteristics of the giant dipole resonance (GDR): (i) its width, (ii) its shape, and (iii) the integrated yield of emitted γ rays in ^{120}Sn and ^{208}Pb as a function of temperature T. The double-time Green's function method has been used to derive a complete set of equations, which allow one to calculate explicitly the GDR width due to coupling to all forward-going processes up to two-phonon ones at most in the second order of the interaction strength. The numerical calculations have been performed using the single-particle energies defined from the Woods-Saxon potentials. An overall agreement between theory and experiment is found for all three characteristics. The results show that the total width of the GDR due to coupling of the GDR phonon to all ph, pp, and hh configurations increases sharply at low temperatures up to $T\sim$ 3 MeV and saturates at $T\sim 4$–6 MeV. The quantal width Γ_Q due to coupling to ph configurations decreases slowly with increasing T. It becomes almost independent of T only when the contribution of two-phonon processes at $T\neq 0$ is omitted. The observed saturation of the integrated yield above $E^*\sim 300$ MeV is reproduced in both the GDR region and the region above it. [S0556-2813(98)03812-6]

PACS number(s): 21.10.Pc, 24.10.Pa, 24.30.Cz

I. INTRODUCTION

The giant dipole resonance (GDR) is one of the most spectacular and best known results of nuclear physics. It is generated by the collective motion of protons against neutrons in a nucleus. Apart from the GDR built on the ground state (g.s. GDR), the GDR built on compound nuclear states (hot GDR) has been the subject of a considerable number of experimental and theoretical studies during the past 15 years (see Refs. [1] and [2] for reviews).

The width of the g.s. GDR consists mainly of the Landau damping width (Landau splitting) σ, the escape width $\Gamma^{\uparrow}$, and the spreading width $\Gamma^{\downarrow}$. The Landau splitting σ represents the distribution of the GDR over a number of harmonic oscillators, whose frequencies are scattered around the GDR energy. It can be well described within the random-phase approximation (RPA), in which the GDR is composed of collective particle-hole (ph) vibrational states (phonons). The escape width $\Gamma^{\uparrow}$ arises from the particle emission and can be studied via coupling to the continuum. The value of the escape width $\Gamma^{\uparrow}$ is small (a few hundred keV). The main part of the total width of GDR comes from the spreading width $\Gamma^{\downarrow}$, which the GDR acquires via coupling to complicated configurations such as $2p2h$ and even more complex ones. In such microscopic descriptions as the quasiparticle-phonon model [3] or the nuclear-field theory (NFT) [4] the coupling to $2p2h$ configurations is expressed in terms of coupling to two-phonon states [3] or to $1p1h\otimes$phonon states [4]. The most direct $2p2h$-configuration mixing has been performed within the second RPA [5] and its extended version [6]. A simple extension of these microscopic descriptions of the width of the g.s. GDR to nonzero temperature ($T\neq 0$) has shown that all three components of the GDR width depend weakly on temperature [7–10]. This is contradictory to the experimental systematic of the width of hot GDR, which increases rapidly at low excitation energies E^* (or temperature T) [11–18]. At higher excitation energies the observed width increases slowly and even saturates at $E^*\geqslant 130$ MeV in tin isotopes [19,20].

Within the framework of macroscopic approaches including the deformation parameter β the increase of the width at nonzero temperature has been described by taking into account thermal fluctuations of nuclear shapes [21–23]. They were also taken into account in the recent theoretical evaluation in the adiabatic coupling model in Ref. [24]. The adiabatic coupling model interpreted the GDR broadening via adiabatic coupling of the collective vibration to nuclear quadrupole shape fluctuations. It described well the recent data from the inelastic α-scattering experiments in Refs. [17,18] for the GDR width in ^{120}Sn and ^{208}Pb at temperatures 1 MeV $<T\leqslant 3$ MeV (30 MeV $\leqslant E^*\leqslant 130$ MeV). The increase of the evaporation width Γ_{ev} due to a finite lifetime of the compound nuclear states [25] has also been included to improve the results at $T\sim 3$ MeV. The width of the GDR may depend noticeably on the angular momentum J if the latter reaches a rather high value $J\geqslant 35\hbar$ at $T\simeq 1.5$–1.8 MeV in a lighter nucleus ^{106}Sn [26]. Existing calculations within the framework of the cranked Hartree-Fock-Bogolyubov plus thermal RPA theory for the GDR excited on the thermal high-spin states in ^{162,168}Er [27] have shown that the strength function of the hot GDR depends weakly on the angular momentum up to $J=44\hbar$ within the temperature interval $0\leqslant T\leqslant 3$ MeV. The recent experimental evidence in Ref. [18] has also shown that the GDR widths measured in inelastic α-scattering experiments and in fusion reactions do not differ much in their evolution with T while the angular momentum is about 10–20 $\hbar$ lower in the case of the inelastic scattering data. This is a clear indication that the effect of spin on the hot GDR in tin isotopes is not significant. In the colli-

*On leave of absence from the Institute of Nuclear Science and Technique, VAEC, Hanoi, Vietnam. Electronic address: dang@rikaxp.riken.go.jp

sional damping model [28–30] the interplay between one-body Landau damping and two-body collisional damping of nucleons within the linearized Landau-Vlasov theory has been elaborated to study the damping of the hot GDR. This approach described satisfactorily the width increase in ^{208}Pb but underestimated the width in ^{120}Sn by $\sim 20-30\,\%$ within the same temperature region [18].

In the region $T>3$ MeV where the observed width saturates existing models gave different trends for the GDR width. The model proposed by the Milan group in Ref. [31] interpreted the width saturation as a consequence of the limitation of the maximum spin that a compound nucleus could reach. The collisional damping gave a continuously increasing width, which became larger than 20 MeV at $T>3-4$ MeV. With such a large width the existence of the GDR itself becomes questionable. This result is in favor of the disappearance of the GDR at high T. As a matter of fact, in order to fit their data on the saturation of the γ-ray yield in the GDR region in tin isotopes the authors of Ref. [32] also introduced a width in the multistep CASCADE calculations, which increased sharply with increasing T. From this parametrization it was concluded in Ref. [32] that the GDR gradually disappeared at high temperature. However, recent measurements by the MEDEA collaboration [15] have shown that such a large width overestimated strongly the intergated yield of the γ rays in the region above the GDR (20 MeV $\leqslant E_\gamma \leqslant$ 35 MeV) within the same multistep CASCADE calculations. The GDR cross sections estimated using the width parametrizations by the collisional damping model and by Ref. [32] were also strongly enhanced in comparison to the data [16]. Meanwhile, it has also been shown in Ref. [15] that the γ spectra in tin isotopes can be well described using a saturated value of 12 MeV for the GDR width and a cutoff of γ emission from the GDR above $E^* \sim 250$ MeV.

The energy and the full width at the half maximum (FHWM) are only two parameters that reflect the evolution of the hot GDR. The authors of the quite recent Ref. [33] have pointed out that not only the comparison of the calculated FWHM and the experimental GDR width, but also the complete shape of the GDR strength function should be considered to achieve a meaningful comparison between theory and experiment. The detailed analysis in Ref. [33], which included the entire shape of the strength function, has shown that neither the adiabatic coupling model [24] nor the collisional damping model [28–30] could reproduce the observed GDR shape.

Recently, we have proposed an approach to the width of the hot GDR, which has shown that the coupling of the collective dipole vibration (GDR phonon) to the incoherent particle-particle (pp) and hole-hole (hh) configurations appearing at nonzero temperature (the thermal damping) is decisively important for an adequate description of the width increase and its saturation [34–38]. It has been also pointed out that coupling to pp and hh configurations is *de facto* taking shape fluctuations into account [34–36]. At the same time it has been concluded that the quantal damping due to coupling to only ph configurations decreases slowly as the temperature increases. The application of this approach in a systematic study of the quantal and thermal dampings of the hot GDR in ^{90}Zr, ^{120}Sn, and ^{208}Pb has shown reasonable agreement with the experimental data [34,35].

The coupling of the GDR phonon to the single-particle field in Refs. [34,35] has been carried out up to the $2p1h$ level in the mass operator for the single-particle damping. A natural question arises on the contribution of higher-order processes such as $1p1h\otimes$phonon, $1p1p\otimes$phonon, $1h1h\otimes$phonon, or/and two-phonon ones to the GDR width as a function of temperature. These effects are known to lead explicitly to the major part of the spreading width $\Gamma^{\downarrow}$ of the g.s. GDR. The purpose of the present paper is to answer this question. In order to achieve this goal a complete set of approximate equations will be derived including all the forward-going processes up to two-phonon ones at nonzero temperature. The model is tested in numerical calculations of the hot GDR width, its shape, and the integrated yield of the γ rays in ^{120}Sn and ^{208}Pb. The results will be compared with the experimental systematics from Refs. [11,13–20,32,33]. The results will demonstrate that this more refined scheme can serve as a further justification for the conclusions obtained within the simpler scheme in Refs. [34,35]. On the other hand, the present higher-order approximate scheme allows us to shed light on the contribution of different graphs in the hot GDR width as a function of temperature and establish a connection to existing microscopic theories for the damping of the hot GDR such as the extension of NFT to nonzero temperature [9,39]. As the present paper is a further development of the approach in Refs. [34,35], the latter will be frequently referred to for comparison.

The present paper is organized as follows. The complete set of approximate equations of the approach is derived in Sec. II. Section III is devoted to the analysis and discussion of numerical results. The paper is summarized in Sec. IV, where conclusions are provided.

II. FORMALISM

We consider the same model Hamiltonian as in [35] for the description of the coupling of collective oscillations (phonons) to the field of ph, pp, and hh pairs. This Hamiltonian is composed of three terms

$$H=H_a+H_b+H_c\,. \tag{2.1}$$

The first term H_a is the field of independent single particles

$$H_a=\sum_s E_s a_s^\dagger a_s\,, \tag{2.2}$$

where $a_s^\dagger$ and a_s are creation and destruction operators of a particle or hole state with energy $E_s=\epsilon_s-\epsilon_F$, with ϵ_s being the single-particle energy and ϵ_F the Fermi energy. From now on we will call the energy E_s the single-particle energy whenever there is no confusion with ϵ_s. The second term H_b in Eq. (2.1) stands for the phonon field as the field of harmonic oscillators

$$H_b=\sum_q \omega_q Q_q^\dagger Q_q\,, \tag{2.3}$$

where $Q_q^\dagger$ and Q_q are the creation and destruction operators of a phonon with energy ω_q. The last term H_c in Eq. (2.1) describes the coupling between the first two terms

$$H_c = \sum_{s,s',q} F^{(q)}_{ss'} a^\dagger_s a_{s'} (Q^\dagger_q + Q_q). \tag{2.4}$$

The indices s and s' denote the particle (p, $E_p > 0$) or hole (h, $E_h < 0$), while the index q is reserved for the phonon state $q = \{\lambda, i\}$ with multipolarity λ (the projection μ of λ in the phonon index is omitted for simplicity). The sums in Eqs. (2.3) and (2.4) are carried over $\lambda \geqslant 1$ in general.

We make use of the method of the temperature-dependent double-time Green's functions [40–42] to derive a closed set of coupled equations, which describes the damping of the GDR. In [35] the damping of the phonon excitation, which generates the GDR, has been studied using the following double-time Green's functions: (i) *the propagation of a free phonon*

$$G_{q';q}(t-t') = \langle\langle Q_{q'}(t); Q^\dagger_q(t')\rangle\rangle \tag{2.5}$$

and (ii) *the transition between a nucleon pair and a phonon*

$$\mathcal{G}_{ss';q}(t-t') = \langle\langle a^\dagger_s(t) a_{s'}(t); Q^\dagger_q(t')\rangle\rangle. \tag{2.6}$$

The effect of single-particle damping on the GDR width has been found in [35] to be rather small up to high excitation energies. Therefore, we will not consider it here again. In order to study the contribution of the higher-order graphs, let us introduce in addition to Eqs. (2.5) and (2.6) also the double-time Green's functions, which describe the following processes

(iii) *the transition between a* $1p1h \otimes$ phonon ($1p1p \otimes$ *phonon* or $1h1h \otimes$ phonon) configuration and a phonon

$$\Gamma^{-,+}_{ss'q';q}(t-t') = \langle\langle a^\dagger_s(t) a_{s'}(t) Q_{q'}(t); Q^\dagger_q(t')\rangle\rangle \tag{2.7}$$

and (iv) *the transition between two- and one-phonon configurations*:

$$G^{--,+}_{q_1q_2}(t-t') = \langle\langle Q_{q_1}(t) Q_{q_2}(t); Q^\dagger_q(t')\rangle\rangle. \tag{2.8}$$

In Eqs. (2.5)–(2.8) the standard notation for the double-time retarded Green's function is used [41]. In principle, the backward-going processes, described by the Green's functions $G^{+,+}_{q';q}(t-t') = \langle\langle Q^\dagger_{q'}(t); Q^\dagger_q(t')\rangle\rangle$, $\Gamma^{+,+}_{ss'q';q}(t-t') = \langle\langle a^\dagger_s(t) a_{s'}(t) Q^\dagger_{q'}(t); Q^\dagger_q(t'),\rangle\rangle$, and $G^{++,+}_{q_1q_2}(t-t') = \langle\langle Q^\dagger_{q_1}(t) Q^\dagger_{q_2}(t); Q^\dagger_q(t')\rangle\rangle$, also take place. However, if the poles of the forward-going processes in Eqs. (2.5)–(2.8) are located in the region of the GDR, the poles of these backward-going processes will be located at negative energies far away from the GDR region. Hence, just like the Y amplitudes in the RPA, they are not expected to affect noticeably the damping properties of the GDR. Therefore, we will neglect all backward-going processes hereafter to maintain the simplicity.

Applying now the standard method of the equation of motion for the double-time Green's function [41], we obtain a set of coupled equations for a hierarchy of double-time Green's functions. Employing the decoupling approximation discussed previously in [35], we can close the set to the functions in Eqs. (2.5)–(2.8). Making then the Fourier transformation to the energy plane E, we obtain a set of four equations for the Fourier transforms of the Green's functions in Eqs. (2.5)–(2.8), from which three following equations are exact (up to neglecting backward-going processes):

$$(E-\omega_q) G_{q;q}(E) - \sum_{s_1,s'_1} F^{(q)}_{s_1s'_1} \mathcal{G}_{s_1s'_1;q}(E) = \frac{1}{2\pi}, \tag{2.9}$$

$$(E - E_{s'} + E_s)\mathcal{G}_{ss';q}(E) - \sum_{s_1,q'} [F^{(q')}_{s's_1}\Gamma^{-,+}_{ss_1q';q}(E) - F^{(q')}_{s_1s}\Gamma^{-,+}_{s_1s'q';q}(E)] = 0, \tag{2.10}$$

$$(E-\omega_{q_1}-\omega_{q_2}) G^{--,+}_{q_1q_2;q}(E) - \sum_{s,s'} [F^{(q_1)}_{ss'}\Gamma^{-,+}_{ss'q_2;q}(E) + F^{(q_2)}_{ss'}\Gamma^{-,+}_{ss'q_1;q}(E)] = 0. \tag{2.11}$$

The fourth equation is approximated due to the decoupling scheme mentioned above and has the form

$$\begin{aligned}(E - E_{s'} + E_s - \omega_{q'})\Gamma^{-,+}_{ss'q';q}(E) &- (1-n_{s'}+\nu_{q'})\sum_{s_1} F^{(q')}_{s's_1}\mathcal{G}_{ss_1;q}(E) \\ &+ (n_s+\nu_{q'})\sum_{s_1} F^{(q')}_{s_1s}\mathcal{G}_{s_1s';q}(E) \\ &- (n_s - n_{s'})\sum_{q_1} F^{(q_1)}_{s's} G^{--,+}_{q_1q';q}(E) = 0,\end{aligned} \tag{2.12}$$

In Eq. (2.12) the single-particle occupation number n_s and phonon occupation number ν_q occur after applying the decoupling scheme. The explicit equations for these occupation numbers are given in [35], which show that they are Fermi-Dirac and Bose-Einstein distributions, which are smeared out by a half-width of the single-particle and phonon dampings, respectively. Eliminating $\mathcal{G}_{ss';q}(E)$ from Eqs. (2.9) and (2.10), we obtain one exact equation, which relates $G_{q;q}(E)$ to $\Gamma^{-,+}_{ss',q}(E)$, in the form

$$(E-\omega_q) G_{q;q}(E) - \sum_{s,s',s_1,q'} \frac{F^{(q)}_{ss'}[F^{(q')}_{s's_1}\Gamma^{-,+}_{s's_1q';q}(E) - F^{(q')}_{s_1s}\Gamma^{-,+}_{s_1s'q';q}(E)]}{E - E_{s'} + E_s} = \frac{1}{2\pi}. \tag{2.13}$$

Since the evolution of the collective phonon is defined by the propagator $G_{q;q'}(E)$, we have to derive an equation, that contains only one-phonon propagator $G_{q;q'}(E)$ as the unknown. This means that we must find the way to estimate the Green's function $\Gamma^{-,+}(E)$ in Eq. (2.13) in terms of $G_{q';q}(E)$. This goal can be achieved making use of the two Eqs. (2.11) and (2.12). Eliminating $G^{--,+}_{q_1q_2;q}(E)$ by expressing it in terms of $\Gamma^{-,+}(E)$ using Eq. (2.11) and inserting the result into Eq. (2.12), we arrive at the following approximate equation, which relates the functions $\Gamma^{-,+}(E)$ to $\mathcal{G}_{ss',q}(E)$:

$$(E-E_{s'}+E_s-\omega_{q'})\Gamma^{-,+}_{ss';q'q}(E)$$
$$=(1-n_{s'}+\nu_{q'})\sum_{s_1} F^{(q')}_{s's_1}\mathcal{G}_{ss_1;q}(E)-(n_s+\nu_{q'})$$
$$\times\sum_{s_1} F^{(q')}_{s_1s}\mathcal{G}_{s_1s';q}(E)+(n_s-n_{s'})$$
$$\times\sum_{s_1,s_1',q_1}\frac{F^{(q_1)}_{s's}[F^{(q_1)}_{s_1s_1'}\Gamma^{-,+}_{s_1s_1'q';q}(E)+F^{(q')}_{s_1s_1'}\Gamma^{-,+}_{s_1s_1'q_1;q}(E)]}{E-\omega_{q_1}-\omega_{q'}}. \tag{2.14}$$

Making again the decoupling for all the Green's functions under the sums on the right-hand side (rhs) of Eq. (2.14), which truncates the chain at $O((F^{(q')}_{ss'})^2)$ of the interaction strength $F^{(q')}_{ss'}$, we can express $\Gamma^{-,+}_{ss';q'q}(E)$ in terms of $G_{q',q}(E)$ as

$$(E-E_{s'}+E_s-\omega_{q'})\Gamma^{-,+}_{ss';q'q}(E)=\sum_{q_1}\mathcal{M}^{q_1q'}_{ss'}(E)G_{q_1;q}(E). \tag{2.15}$$

Inserting $\Gamma^{-,+}_{ss';q'q}(E)$ from the approximate equation (2.15) into the exact equation (2.13), we end up with the final equation for the propagation of a single phonon ($q_1=q$) in the form

$$G_{q,q}(E)=\frac{1}{2\pi}\frac{1}{E-\omega_q-P_q(E)}. \tag{2.16}$$

The explicit expressions of the polarization operator $P_q(E)$ and the shorthand vertex function $\mathcal{M}^{q_1q'}_{ss'}(E)$ in Eqs. (2.15) and (2.16) are

$$P_q(E)=\sum_{s,s',s_1,q'}\frac{F^{(q)}_{ss'}}{E-E_{s'}+E_s}\left[\frac{F^{(q')}_{s's_1}\mathcal{M}^{qq'}_{ss_1}(E)}{E-E_{s_1}+E_s-\omega_{q'}}-\frac{F^{(q')}_{s_1s}\mathcal{M}^{qq'}_{s_1s'}(E)}{E-E_{s'}+E_{s_1}-\omega_{q'}}\right], \tag{2.17}$$

$$\mathcal{M}^{qq'}_{ss'}(E)=\sum_{s_2}\left\{\frac{(1-n_{s'}+\nu_{q'})(n_s-n_{s_2})}{E-E_{s_2}+E_s}F^{(q')}_{s's_2}F^{(q)}_{s_2s}-\frac{(n_s+\nu_{q'})(n_{s_2}-n_{s'})}{E-E_{s'}+E_{s_2}}F^{(q')}_{s_2s}F^{(q)}_{s's_2}+n_{s_2}(n_s-n_{s'})\times\left[\frac{F^{(q)}_{s's}F^{(q')}_{s_2s_2}}{E-\omega_q-\omega_{q'}}+\delta_{qq'}\sum_{q_1}\frac{F^{(q_1)}_{s's}F^{(q_1)}_{s_2s_2}}{E-\omega_{q_1}-\omega_{q'}}\right]\right\}. \tag{2.18}$$

The merit of this approximation scheme is twofold. It allows one to take explicitly into account all the forward-going processes with $1p1h\otimes$phonon, $1p1p\otimes$phonon, and $1h1h\otimes$phonon as well as two-phonon configurations rather than including them effectively in the parameters of the model in [35]. At the same time it is simple enough for a straightforward evaluation of the damping of the hot GDR to become feasible. Indeed, as has been discussed in [35], the damping width Γ_{GDR} of the hot GDR located at energy $\omega=\omega_{GDR}$ is defined via the imaginary part of the analytical continuation of the polarization operator $P_q(E)$ into complex energy plane $E=\omega\pm i\varepsilon$ as

$$\Gamma_{GDR}=2\gamma_q(\omega)|_{\omega=\omega_{GDR}}=2|\mathrm{Im}P_q(\omega\pm i\varepsilon)|_{\omega=\omega_{GDR}}. \tag{2.19}$$

The energy ω_{GDR} of the hot GDR is defined as the solution $\overline{\omega}$ of the following equation for the pole of the Green's function in Eq. (2.16):

$$\omega-\omega_q-P_q(\omega)=0, \tag{2.20}$$

where $P_q(\omega)$ (ω is real) is the real part of $P_q(E)$.

It has been shown in [35] that the coupling to pp and hh configurations appearing at $T\neq 0$ leads to the increase of the width at low T and its saturation at high T. The reason is in the factor $n_p-n_{p'}$ (and $n_h-n_{h'}$), which appeared in the polarization operator $P_q(E)$ as a result of averaging over the grand canonical ensemble [see Eqs. (2.17) and (2.18) above and also Eqs. (3) and (5) of Ref. [34]]. This factor increases first with increasing T, but decreases as $O(T^{-1})$ at large T. Therefore, it must reach some plateau within a certain region of temperature. This plateau corresponds to the region of the width saturation. It has also been shown that this mechanism of coupling to pp and hh configurations is a microscopic way to take into account shape fluctuations. This essential difference from the summation of over only n_h-n_p is due to the fact that a pp or an hh pair can be expanded into a sum of tensor products of two ph pairs. If the total multipolarity and parity of the tensor product is 1^- as of the GDR, the two ph pairs can take the multipolarities and parities as $(2^+,1^-)$, $(3^-,2^+)$, etc. This means that not only the quadrupole vibrations, but also higher multipolarities are effectively taken into account in the coupling to pp and hh configurations. Since this matter has been discussed previously, we will not repeat here again, referring to [35] for more details. This mechanism remains unchanged in the present more refined approximation, which replaces an effective account for doorways via selecting the parameters at $T=0$ with an explicit specification of doorways as all forward-going configurations up to two-phonon ones.

The graphs, included in the present approximation scheme, are depicted in Figs. 1(a)–1(e). The graphs in Fig. 1(a)–1(d) are summed up in Eq. (2.17), where only the first two terms on the rhs of Eq. (2.18) are taken into account. The graph in Fig. 1(e) is due to the last two terms on the rhs of Eq. (2.18). Therefore, the polarization operator $P_q(E)$ contains not only $1p1h$ and $1p1h\otimes$phonon graphs as in the NFT [4,9] [Figs. 1(f)–1(i)], but also $1p1p$, $1h1h$, $1p1p\otimes$phonon, and $1h1h\otimes$phonon graphs [Fig. 1(a)–1(d)]. Moreover, it includes also the graph in Fig. 1(e) due to the two-phonon process in Eq. (2.8) at the same second order in

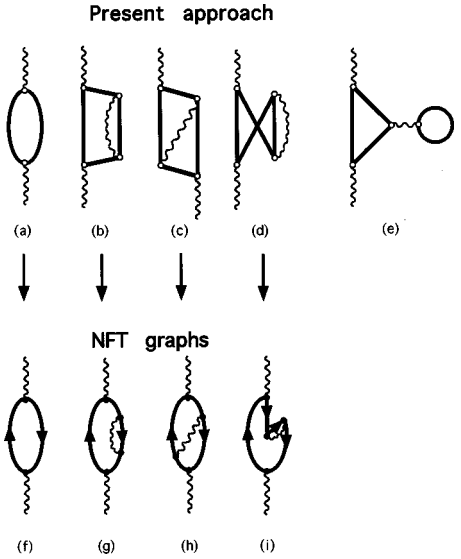

FIG. 1. (a)–(e): Graphs included in the present formalism. (f)–(i) NFT graphs. A wavy line denotes a phone line, while a solid line stands for a single-particle line (particle or hole). An open circle denotes the interaction vertex $F^{(q)}_{ss'}$. In (f)–(i) a pair of solid lines with arrows going in and out of an interaction vertex (closed circle) describes a ph pair interacting with a phonon.

the interaction strength. In the limit of high temperature it is easy to see that the vertex function $\mathcal{M}^{qq'}_{ss'}(E)$ in Eqs. (2.17) and (2.18) tends to

$$\mathcal{M}^{q_1q'}_{ss'}(E)|_{T\to\infty}\to\frac{1}{4}\sum_{s_2}\left\{\frac{1}{\omega_{q'}}\left[\frac{E_{s_2}-E_s}{E-E_{s_2}+E_s}F^{(q')}_{s's_2}F^{(q)}_{s_2s}+\frac{E_{s_2}-E_{s'}}{E-E_{s'}+E_{s_2}}F^{(q')}_{s_2s}F^{(q)}_{s's_2}\right]+\frac{1}{2T}(E_{s'}-E_s)\left[\frac{F^{(q)}_{s's}F^{(q')}_{s_2s_2}}{E-\omega_q-\omega_{q'}}+\delta_{qq'}\sum_{q_1}\frac{F^{(q_1)}_{s's}F^{(q_1)}_{s_2s_2}}{E-\omega_{q_1}-\omega_{q'}}\right]\right\}, \quad (2.21)$$

which means that it decreases as $O(T^{-1})$ with increasing T because of the factor T^{-1} in front of two-phonon terms on the rhs of Eq. (2.21). Neglecting these two-phonon processes [the graph in Fig. 1(e)] would lead to a constant width at high temperature because the first two terms on the rhs of Eq. (2.21) are independent of T under the assumption that the temperature dependence of the interaction, of the phonon energy, and of the difference $E_{s'}-E_s$ is negligible. The decrease of the quantal width of the GDR as $O(T^{-1})$ at high T has been also estimated analytically in the second RPA in Ref. [43].

The shape of the GDR is described by the strength function $S^{GDR}_q(\omega)$, which is is related to the spectral intensity $J_q(\omega)$. The latter has been derived in the standard way using the analytic continuation of the Green's function $G_q(\omega\pm i\varepsilon)$ [40] as

$$J_q(\omega)=\frac{1}{\pi}\frac{\gamma_q(\omega)[e^{(\omega/T)}-1]^{-1}}{(\omega-\omega_q-P_q(\omega))^2+[\gamma_q(\omega)]^2}. \quad (2.22)$$

As has been shown in Ref. [36], the total divided strength distribution $J_q(\omega)[\exp(\omega/T)-1]$ calculated from Eq. (2.22) is similar to the experimentally extracted GDR shape only at very low temperatures. The increase of thermal fluctuations leads to a gradual enhancement of the wings of this strength distribution with increasing T. Within the concept of many-body quantum chaos [44] this corresponds to a transition of the strength function from the regime of the ''standard model'' with weakly fluctuating matrix elements to the stochastic regime. In this case the usual estimation of the width via the energy variance based on this total strength distribution is no longer reliable [36]. In our approach the GDR width is defined as in Eq. (2.19), which is the FWHM of the GDR peak located at ω_{GDR}. Consequently, the strength function of the GDR suitable for a direct comparison with the experimental data must be defined as the one of the damped GDR phonon with energy $\overline{\omega}$, which is shifted from ω_q as the solution of Eq. (2.20). The simplest approximation for this strength function can be obtained, noticing that the spectral intensity $J_q(\omega)$ in Eq. (2.22) has a steep maximum at this pole $\overline{\omega}$. Expanding the polarization operator $P_q(\omega)$ in a power series in ω near this pole and keeping only the lowest order of this expansion, we arrive at the approximation $S^{GDR}_q(\omega)$ for the hot GDR strength function

$$S^{GDR}_q(\omega)=\frac{1}{\pi}\frac{\gamma_q(\omega)}{(\omega-\overline{\omega})^2+[\gamma_q(\omega)]^2}. \quad (2.23)$$

As the damping $\gamma_q(\omega)$ depends on the energy variable ω, which runs over the γ-ray energy E_γ, the shape of the strength function $S^{GDR}_q(\omega)$, strictly speaking, is not given by a single Breit-Wigner curve. This strength function $S^{GDR}_q(\omega)$ can be directly compared with the divided spectra in the linear scale normalized by a strength constant, while the corresponding spectral intensity

$$J^{GDR}_q(\omega)=\frac{S^{GDR}_q(\omega)}{e^{\omega/T}-1} \quad (2.24)$$

is proportional to the exponential shape of the γ-ray spectra observed in experiments. It is also worth noticing that the Fourier transform of the spectral intensity $J^{GDR}_q(\omega)$ defines the time correlation function, which allows one to study directly the relaxation process and the coexistence of orders and chaos in the phenomenon of the hot GDR. This issue is now being studied by us and we plan to report the results in a forthcoming paper.

The present formalism considers the hot GDR, its width, and shape as a result of averaging over the grand canonical ensemble at a given temperature. Therefore, the yield of the γ ray can be calculated here following the standard statistical model using simplifying assumptions. They included a T^2

dependence for the neutron-decay width and the first order of the logarithmic expansion of the level density [45]. This allows us to calculate the integrated yield Y_γ within the interval $E_1 \leqslant \omega \leqslant E_2$ as

$$Y_\gamma \propto \frac{1}{T^2}\int_{E_1}^{E_2} \omega^3 J_q^{GDR}(\omega) e^{(B_n/T)} d\omega, \qquad (2.25)$$

where B_n represents the neutron binding energy and $J_q^{GDR}(\omega)$ is the spectral intensity defined in Eq. (2.24). This quantity should be compared with the empirically extracted yield, where a Lorentzian strength function $f_{GDR}(\omega)$ multiplied by $\exp(-\omega/T)$ was used instead of $J_q^{GDR}(\omega)$ [1]. We have checked that in the region of the GDR peak a Lorentzian distribution centered at ω_{GDR} with a FWHM Γ_{GDR} has almost the same shape as the Breit-Wigner one divided by ω_{GDR} with the same width.

III. NUMERICAL RESULTS

A. Selection of parameters of the model

In this section we present the results of the calculations of the GDR width Γ_{GDR} according to Eq. (2.19), its strength function $S_q^{GDR}(\omega)$ defined in Eq. (2.23), and the integrated yield Y_γ of γ rays from Eq. (2.25) for ^{120}Sn and ^{208}Pb as a function of temperature within the interval $0 \leqslant T \leqslant 6$ MeV. For this purpose we employ the same model, which has been used previously in [35]. According to this model, the g.s. GDR is generated by a single collective and structureless phonon width energy ω_q closed to the energy ω_{GDR} of the g.s. GDR. We employ realistic single-particle energies, calculated in the Woods-Saxon potentials at $T=0$ for ^{120}Sn and ^{208}Pb. The parameters of these potentials have been defined in Ref. [46]. The levels near the Fermi surface for ^{208}Pb are replaced with the empirical ones. The calculations in Ref. [24] have shown that the major contribution of the shape fluctuations in the increase of the GDR width at $T \neq 0$ comes from the quadrupole shape fluctuations. In the present numerical test we retain only dipole and quadrupole phonons in the two-phonon configuration mixing for simplicity, although this is not the restriction of our formalism in general. Consequently, from the sums on the rhs of Eqs. (2.17) and (2.18) there remain only one dipole phonon with $q=q'$, which corresponds to the GDR ($\lambda=1$) and one quadrupole phonon with q_1, which corresponds to the energy of 2_1^+ state ($\lambda=2$). Let us now discuss the selection of parameters used in numerical calculations in more detail. In the simpler approximation scheme of [35] reasonable agreement between theory and data has been achieved via coupling of GDR phonon to all ph, pp, and hh configurations, using the phonon energy ω_q and the matrix elements of the coupling to ph and pp or hh $F_{ph}^{(q)}=F_1$ for $(s,s')=(p,h)$ and $F_{pp}^{(q)}=F_{hh}^{(q)}=F_2$ for $(s,s')=(p,p')$ or (h,h') as parameters. Even though the higher-order graphs were not included in the equations but rather averaged out by the decoupling scheme in [35], this procedure implies that their effects are incorporated effectively in the parameters F_1 and F_2. Since the nucleon-pair $\otimes$phonon and two-phonon graphs are included explicitly in the present paper, the values of the multipole matrix elements $F_{ph}^{(q)}=F_1^{(\lambda)}$ and $F_{pp}^{(q)}=F_{hh}^{(q)}=F_2^{(\lambda)}$ are not the same as in [35] and must be defined for each multipolarity $\lambda=1$ and 2. In order to test the stability of the conclusions the calculations in the present paper have been carried out using two following procedures of selecting parameters, which will be referred to as procedures 1 and 2, respectively. In procedure 1 the empirical values ω_{GDR} of the GDR energy and $\omega_{2_1^+}$ of the 2_1^+ state are used for ω_q and ω_{q_1}, respectively. The values of $F_1^{(\lambda)}$ and $F_2^{(\lambda)}$ ($\lambda=1$ and 2) are selected to restore the results of theoretical prediction for the total width Γ_{GDR} obtained in [35]. The width Γ_{GDR} is calculated at $\omega=\omega_q$. The principle of procedure 2 has been discussed in detail in I. In order to apply this, we first set the ratio $r=F_i^{(2)}/F_i^{(1)}(i=1,2)$ and choose ω_{q_1} in Eq. (2.18) to be close to $\omega_{2_1^+}$. The values of ω_q in Eq. (2.18) and of $F_1^{(1)}$ are then selected in such a way that the solution $\bar{\omega}$ of the equation for the pole of the Green's function in Eq. (2.16) is equal to the GDR energy $\bar{\omega}=\omega_{GDR}$, while the total width $\Gamma_{GDR}(\bar{\omega})$ from Eq. (2.19) reproduces the empirical width of the GDR at $T=0$. The value of $F_2^{(1)}$ is chosen so that $\bar{\omega}$ is stable while the temperature is varied. The best sets of selected parameters are displayed in Table I, parts (a) and (b), for procedures 1 and 2, respectively. Their values do not depend on temperature. This ensures that all thermal effects come from the microscopic configuration mixings, but not from varying parameters. Using these parameters in ^{120}Sn gives the fluctuations in $\bar{\omega}$ within the range of $\Delta\bar{\omega}=\bar{\omega}-\omega_{GDR} \simeq \pm 0.3$ MeV, while in ^{208}Pb, $\Delta\bar{\omega} \simeq \pm 0.1$ MeV. The values of these parameters differ noticeably from those in [35], because the effects of higher-order graphs are now explicitly included in the equations of the formalism. The calculations have used a value equal to 0.5 MeV for the smearing parameter ε in Eq. (2.19). The results have been checked to be stable against varying ε within the interval 0.2 MeV $\leqslant \varepsilon \leqslant$ 1.0 MeV.

TABLE I. Parameters of the model used in the calculations. The values selected following procedure 1 (see the text) are displayed in (a). Those obtained following procedure 2 are shown in (b).

	ω_q (MeV)	$F_1^{(1)}$ (MeV)	$F_2^{(1)}$ (MeV)	r
		(a)		
^{120}Sn	15.40	4.232×10^{-3}	1.840×10^{-1}	1.0×10^{-1}
^{208}Pb	13.65	2.7×10^{-3}	1.0×10^{-1}	8.8×10^{-1}
		(b)		
^{120}Sn	17.0	6.261×10^{-3}	1.845×10^{-1}	8.603×10^{-2}
^{208}Pb	13.8	2.7×10^{-3}	9.95×10^{-2}	8.8×10^{-1}

B. GDR width

The total widths Γ_{GDR} for the hot GDR in ^{120}Sn and ^{208}Pb, calculated from Eq. (2.19) as a function of temperature, are shown by the solid curves in Figs. 2 and 3, using parameters selected from procedures 1 and 2, respectively. The most recent data from the inelastic α-scattering experiments [17] as well as the heavy-ion fusion data in the region of width saturation in tin isotopes [11,13,19,20] are also shown for comparison. The excitation energy E^* from the fusion data has been translated to temperature using the level density parameter $\sim A/8$ as has been adopted in these experi-

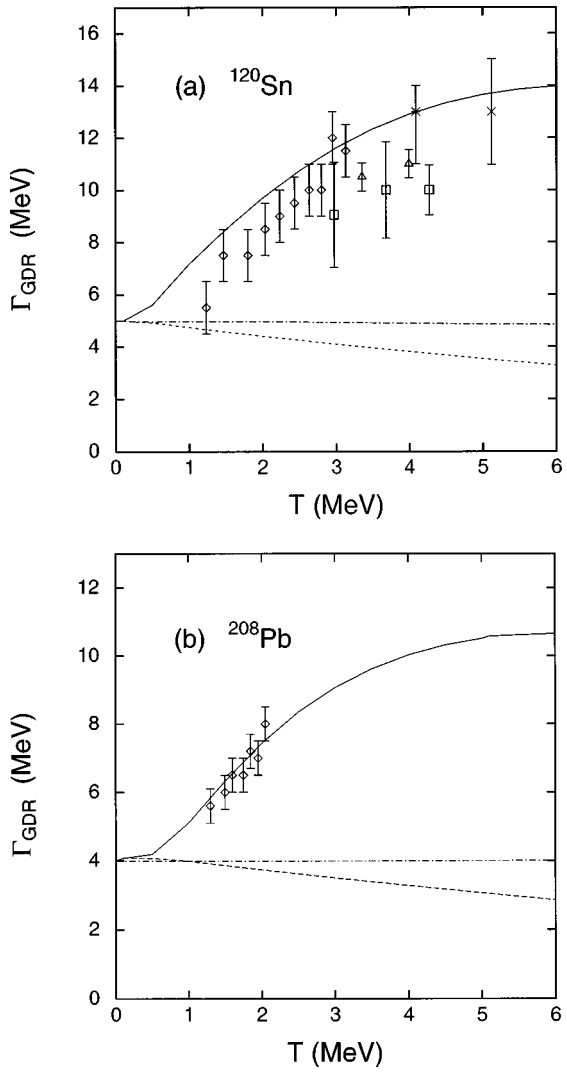

FIG. 2. Width of GDR as a function of temperature for (a) ^{120}Sn and (b) ^{208}Pb. Results have been obtained in the calculations using the parameters in Table I(a). The solid curve denotes the total width Γ_{GDR}. The dashed curve denotes the quantal width Γ_Q. The dash-dotted curve stands for the quantal width Γ_Q when the contribution of the two-phonon processes at $T \neq 0$ is omitted. Diamonds denote the data from Ref. [17]; squares data from Ref. [19]; triangles data from Ref. [20], the cross data from Ref. [11], and the asterisk data from Ref. [13].

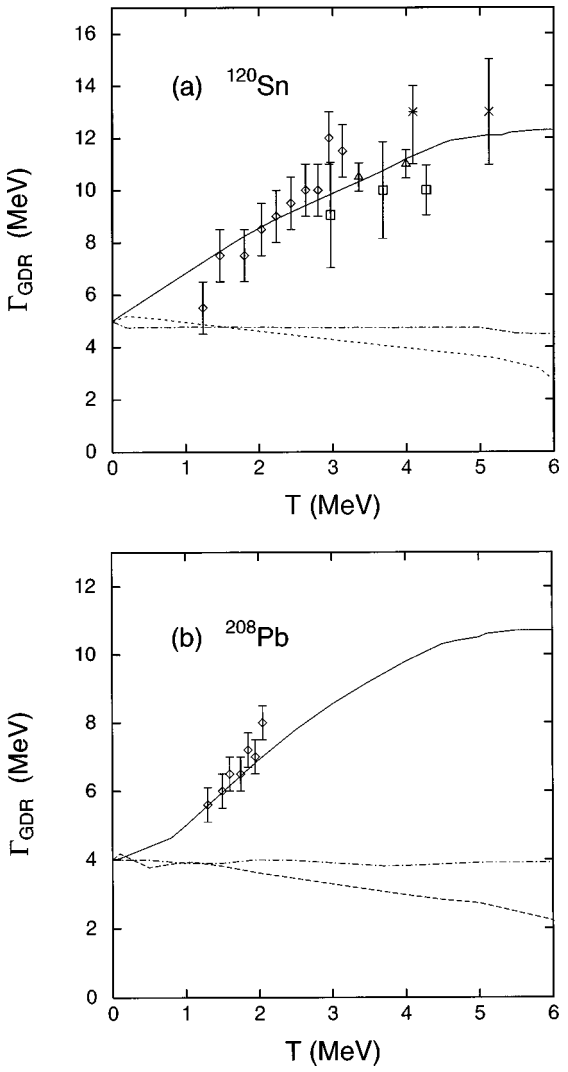

FIG. 3. Results for the same quantities as in Fig. 2, but obtained using the parameters in Table I(b). The notation is the same as in Fig. 2.

mental works. The nice agreement with the data in Fig. 2 is explained by the principle of procedure 1, although in Fig. 3 overall agreement between theory and experiment is also found. In both nuclei the region of width's saturation is at around $T \sim 4-6$ MeV. In ^{208}Pb the saturated value of the width is around 10.5–11 MeV. In ^{120}Sn the uncertainty in the saturated value of the width is somewhat larger because of larger fluctuations in the position of the GDR defined from Eq. (2.20). Nonetheless, this value is about 12–14 MeV, i.e., within the error bars of the data from the heavy-ion fusion experiments [11–16]. A slightly smaller value of the saturated width in ^{120}Sn, which has been obtained using the parameters in Table I(b), as compared to the one obtained in [35], is explained by the fact that only coupling to the quadrupole vibration is considered here. Within the temperature interval $3 \leqslant T \leqslant 5$ MeV this difference is at most around 2 MeV for ^{120}Sn and around 0.8 MeV for ^{208}Pb. More details in confronting the theoretical prediction within this formalism and the data including the region of width saturation can be found in Refs. [34,35]. In these references it has also been discussed thoroughly on the uncertainty in the experimentally extracted temperature from the excitation energy, which makes the comparison between theory and experiment sometime difficult.

As has been demonstrated in [35], the total width Γ_{GDR} is composed of the quantal width Γ_Q due to coupling of the GDR phonon to ph configurations and the thermal width Γ_T due to coupling to pp and hh configurations at $T \neq 0$. The main conclusion of [35] is that the behavior of the total width at high temperatures is mostly driven by the thermal width Γ_T since the quantal width Γ_Q decreases as temperature increases. In order to see whether this conclusion still holds within the present more refined approximation, which includes higher-order processes up to two-phonon ones, we have also switched off the coupling to pp and hh configurations in the sums on the rhs of Eqs. (2.17) and (2.18). The results obtained are shown by the dashed curves in Figs. 2 and 3. They restore perfectly the results for quantal width Γ_Q

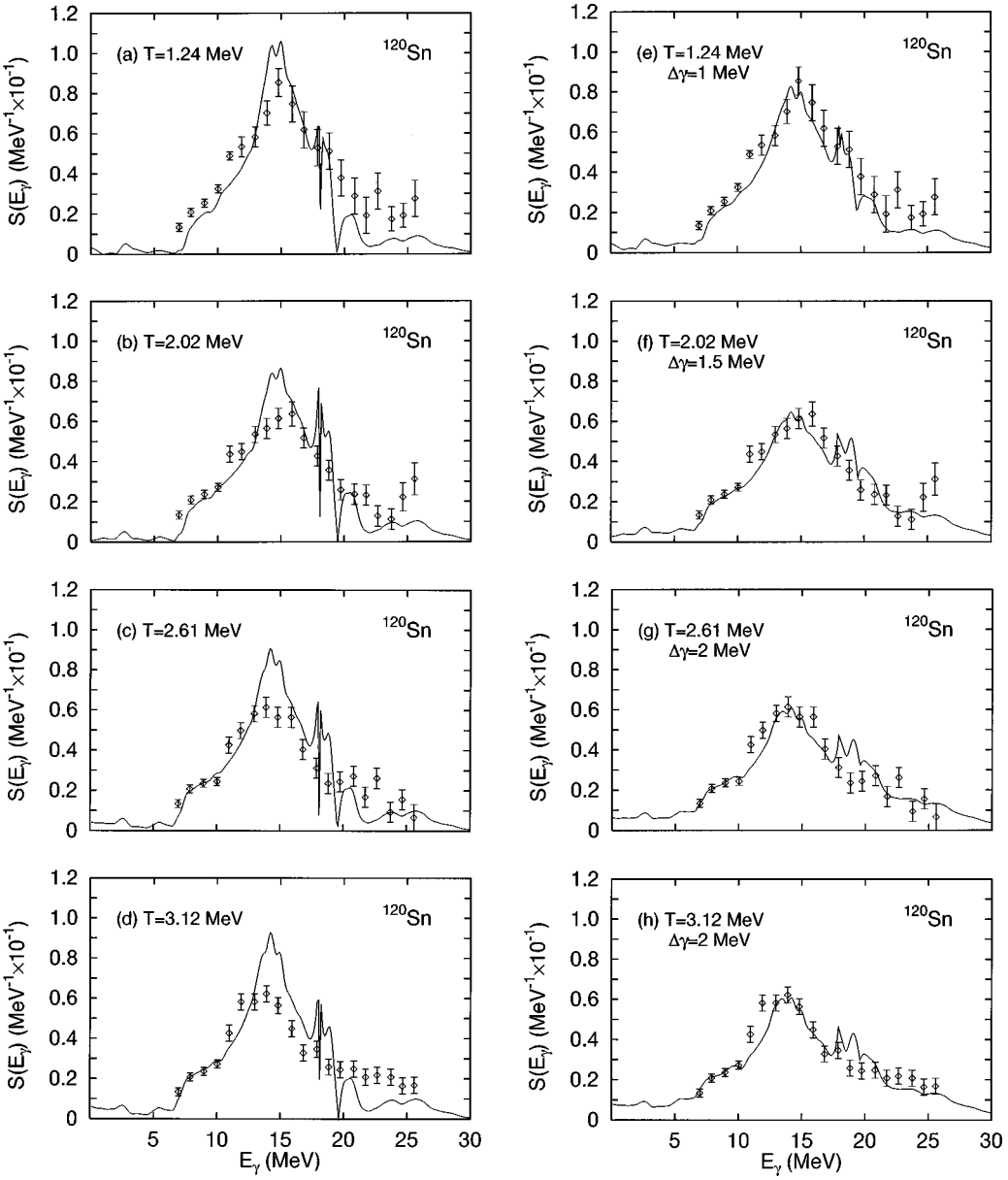

FIG. 4. GDR strength function $S_q^{GDR}(E_\gamma)$ in ^{120}Sn at several temperatures. The solid curve denotes the results of calculations in the present work and diamonds the normalized data from Ref. [18]. In (e)–(h) the results of calculations using $\gamma_q(\omega)+\Delta\gamma$ instead of $\gamma_q(\omega)$ are shown with the corresponding values of $\Delta\gamma$.

in [35], which show a clear decrease as the temperature increases. At $T\sim 5$ MeV the actual value of the quantal width Γ_Q amounts to about 65% of its value at $T=0$.

In order to make the answer to the question on the temperature dependence of the quantal width Γ_Q more definitive it is worthwhile to clarify the relationship between the temperature dependence of the quantal width Γ_Q within the present approach and the one from the NFT at nonzero temperature [9,39]. As has been mentioned in Sec. II, in calculating the quantal width Γ_Q alone, our approach includes also two-phonon processes in parallel with the $ph\otimes$phonon ones, while only the latter were taken into account within the NFT. As a matter of fact, switching off the two-phonon terms at $T\neq 0$ from Eq. (2.18) in the calculation of the width Γ_Q has resulted in a quantal width, that is practically independent of temperature as shown by the dash-dotted curves in Figs. 2 and 3, in agreement with the conclusion within the NFT at $T\neq 0$ [9,39]. These results show that the NFT indeed includes the graphs, which are most important for an adequate description of the quantal width Γ_Q at zero temperature, namely, the $1p1h\otimes$phonon ones. These graphs are a part of the graphs in Figs. 1(a)-1(d) when the summation is carried only over intermediate $1p1h$ and phonon lines [Figs. 1(g)–1(i)]. However, in its extension to nonzero temperature, the NFT neglects entirely the coupling to two-phonon configurations in the vertex function $\mathcal{M}$ in Eq. (2.18) at $T\neq 0$, which enter in the same second order of the interaction strength $F_{ss'}^{(q)}$ and lead to the graph in Fig. 1(e). The importance of these two-phonon processes at $T\neq 0$ is demonstrated here in favor of the conclusion in [35], which states that the quantal width decreases, although slowly, with increasing temperature. Finally, it is important to stress that the NFT at nonzero temperature does not take into account the coupling of pp and hh configurations to phonon ones [the graphs in Figs.

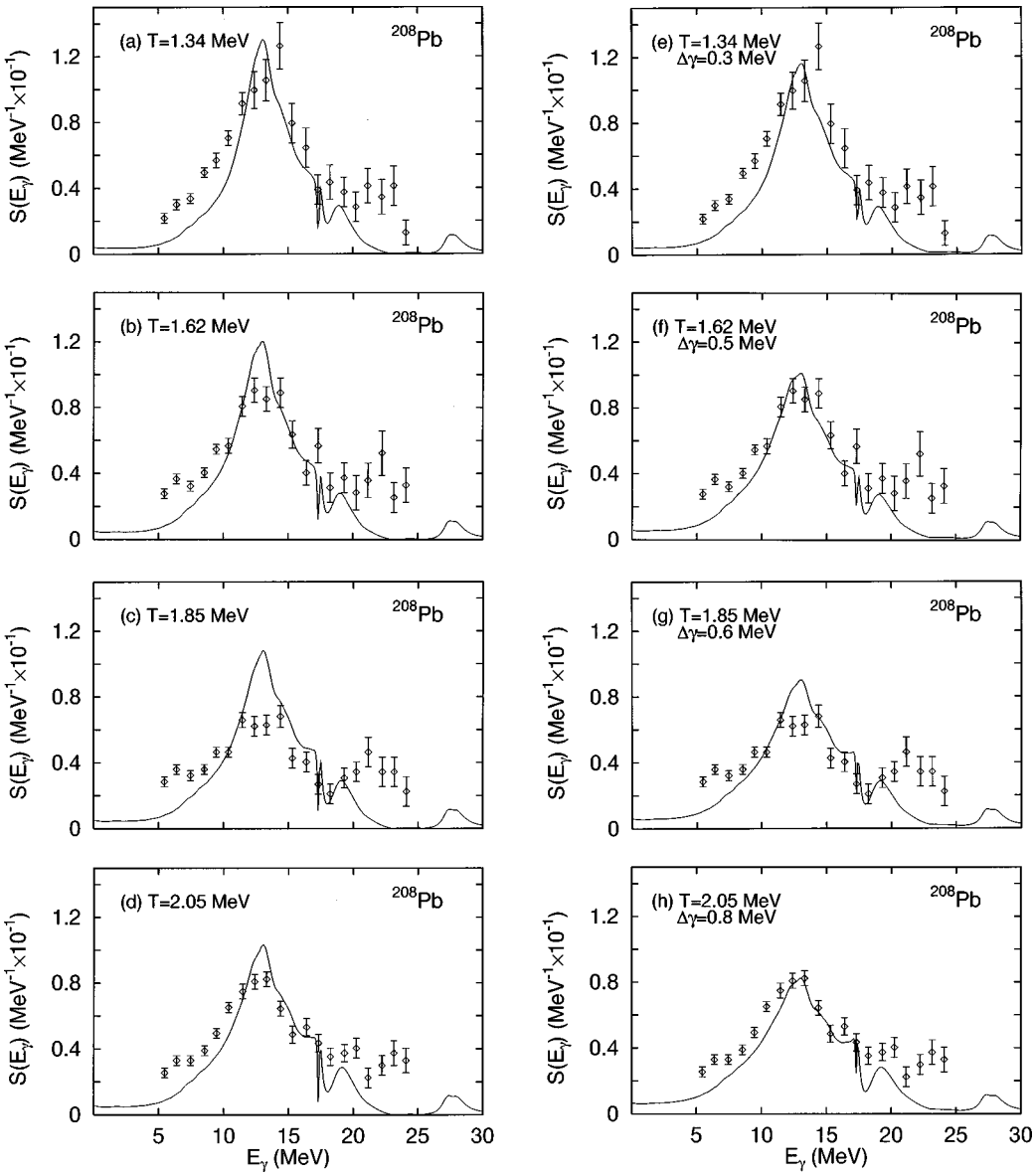

FIG. 5. GDR strength function $S_q^{GDR}(E_\gamma)$ in ^{208}Pb at several temperatures. The notation is the same as in Fig. 4.

1(a)–1(d) with the summation carried over intermediate $1p1p$, $1h1h$, and phonon lines], which is essential for reproducing the width's increase and saturation of the hot GDR. As a matter of fact, the RPA equation at $T\neq 0$ was solved within the NFT [Eq. (24) in Ref. [9]] with the sum carried only over $n_h - n_p$.

An alternative inclusion of shape fluctuations to describe the width's increase in the adiabatic limit has been considered recently in Ref. [24], which may correspond to the lowest-order expansion of the coupling to pp and hh configurations in the present paper in terms of sums of tensor products of two ph pairs, one of which is coupled to the total angular momentum 2^+ and the other one to 1^-, as has been mentioned previously. The applicability of the model in Ref. [24] is restricted by the adiabatic-coupling limit. This may serve as the reason why it can describe the data reasonably well at low temperatures ($T\leqslant 3$ MeV), but still gives a continuously increasing width with increasing T even in the region where the width's saturation has been experimentally observed and where the adiabatic limit should be replaced with the sudden-time limit [36]. The inclusion of only quadrupole shape fluctuations may also lead to a different shape of the strength distribution of the hot GDR in comparison with the experimentally extracted one, as has been discussed recently in Ref. [33]. The formalism of the present paper is free from both of these restrictions.

C. GDR shape

The two sets of selected parameters in the procedures 1 and 2 discussed above did not lead to a significant difference in the evolution of the hot GDR shape as a function of T. Therefore, we will discuss hereinafter the results obtained using the parameters from procedure 2 [Table I(b)].

The results of calculations of the GDR strength function $S_q^{GDR}(\omega)$ are compared with its experimental normalized values $f_{E1}(E_\gamma)$ [18] in the left columns [(a)–(d)] of Fig. 4 for ^{120}Sn and Fig. 5 for ^{208}Pb. The experimentally extracted values of E_γ have been shifted up by 1.5 MeV in ^{120}Sn and by 1 MeV in ^{208}Pb in order to achieve the best agreement.

This is due to the fact that our model assumes a temperature-independent GDR energy ω_{GDR} equal to the energy of the g.s. GDR. The solution $\bar{\omega}$ of Eq. (2.20) has been found to be stable around 15.4 MeV for ^{120}Sn and 13.5 MeV for ^{208}Pb at all temperatures. Meanwhile the experimental resonance energy was found in Ref. [18] to be lower than the g.s. GDR energy by an amount roughly equal to this shift. In other measurements the g.s. GDR energy ($T=0$) has been used for the best fit of the data at $T\neq 0$ [11,13–16,26,32]. At present, no systematic dependence of the GDR energy on the excitation energy E^* (or temperature T) has been confirmed and more studies are called for to resolve this issue. Therefore, we do not consider it reasonable at this stage to vary the parameters of our model with temperature to achieve the decrease of the GDR energy in Ref. [18]. Including this energy shift in the comparison, reasonable agreement between the calculations and the available data is seen for the evolution of the GDR shape in ^{120}Sn (Fig. 4). For ^{208}Pb the data do not strictly follow a Breit-Wigner or Lorentzian shape. At $T=1.85$ MeV the experimental shape of the GDR has even a pronounced structure between 20 and 25 MeV, while the resonance peak seems to be too low. Such particular behavior is not seen in ^{120}Sn or in the gradual change of the calculated shape with increasing T. Additional measurements at this value of T are desirable to clarify this behavior. Nonetheless, the overall agreement between the results of calculations and the data for ^{208}Pb is also satisfactory (Fig. 5).

In order to see a possible improvement of the agreement with the data we notice that since the present test calculations restricts the coupling to ph, pp, and hh configurations via the doorways, which included only dipole and quadrupole phonons, the calculated shape is found to be slightly narrower with a somewhat higher peak. This restriction also caused an enhancement of some structure between 15 and 20 MeV at energies around $\omega_q+\omega_{q_1}$. Taking into account more collective quadrupole phonons and/or phonons of higher multipolarities can improve the agreement. However, it would certainly make the calculations more complicate. At least it would increase the number of the parameters of the model unless the structure of phonon operators is defined microscopically in terms of ph pairs as in the RPA. Incorporating this into the present formalism is another formidable task that we would like to leave for our future studies. In the meantime, a simple way to include effectively the contribution of the missing doorway configurations in the present calculations is adding a parameter $\Delta\gamma$ to $\gamma_q(\omega)$ to minimize the discrepancy between the values of Γ_{GDR} obtained in the present approximation scheme and those obtained in [35]. The strength functions calculated with increasing $\gamma_q(\omega)$ by $\Delta\gamma$ are shown in the right columns [(e)–(h)] of Figs. 4 and 5. By doing so, the overall agreement between theory and experiment is clearly improved. As a prediction of our model we show in Fig. 6 the strength functions of the GDR calculated at several values of $T>4$ MeV in ^{120}Sn and $T\geqslant 2.8$ MeV in ^{208}Pb using $\Delta\gamma=0$ [Figs. 6(a) and 6(b)] as well as $\Delta\gamma=2$ MeV for ^{120}Sn [Fig. 6(c)] and 0.8 MeV for ^{208}Pb [Fig. 6(d)]. The saturation of the GDR shape is clearly seen at $T\geqslant 4$ MeV in both nuclei.

As a visual example of how different models described the experimental data for the GDR shape in ^{120}Sn, we plotted in Fig. 7 the results of our model [(a) and (d)] and those obtained within the adiabatic coupling model [24] [(b) and (e)] and the collisional damping model [30] [(c) and (f)]. The areas of experimental divided spectra as well as the results from the adiabatic coupling and collisional damping models have been taken from Fig. 3 of Ref. [33]. The experimental spectra at low (30–40) MeV and high (110–120 MeV) excitation energies have been rescaled so that they coincide with the data of Ref. [18] at $T=1.24$ MeV [Fig. 4(a) and/or 4(e)] and $T=3.12$ MeV [Fig. 4(d) and/or 4(h)], respectively. It is seen from Fig. 7 that, as compared to the adiabatic coupling and collisional damping models, our approach of-

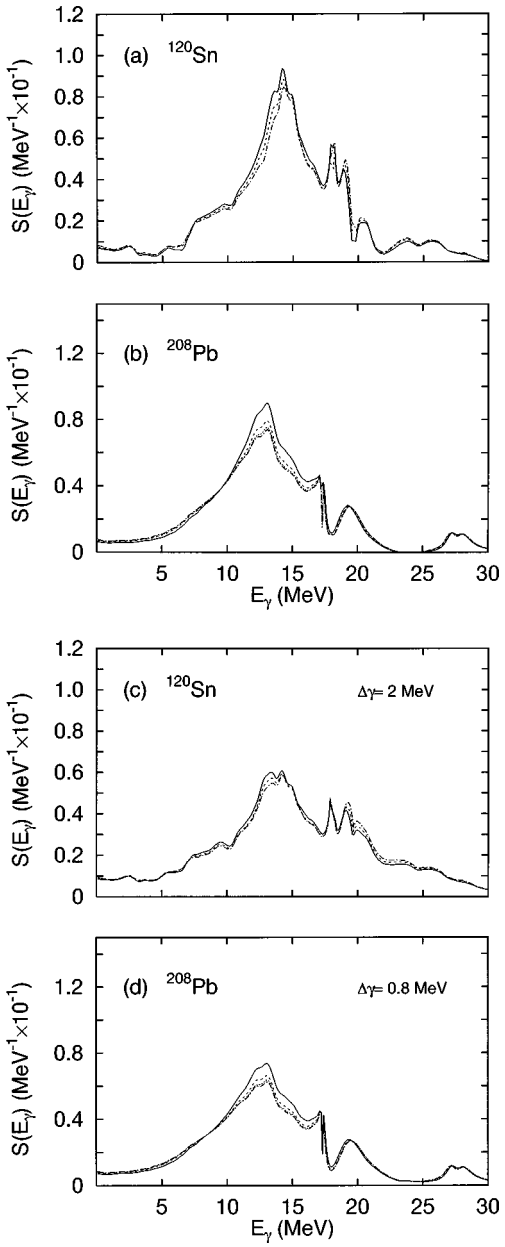

FIG. 6. GDR strength functions $S_q^{GDR}(E_\gamma)$ for (a) and (c) ^{120}Sn and (b) and (d) ^{208}Pb at higher temperatures. In (a) and (c) the solid, dashed, and dash-dotted curves denote the results obtained at $T=4.1$, 5.1, and 5.8 MeV, respectively. In (b) and (d) the solid, dashed, dotted, and dash-dotted curves stand for the results obtained at $T=2.8$, 4, 4.9, and 6 MeV, respectively. The results in (c) and (d) have been obtained using $\gamma_q(\omega)+\Delta\gamma$ instead of $\gamma_q(\omega)$.

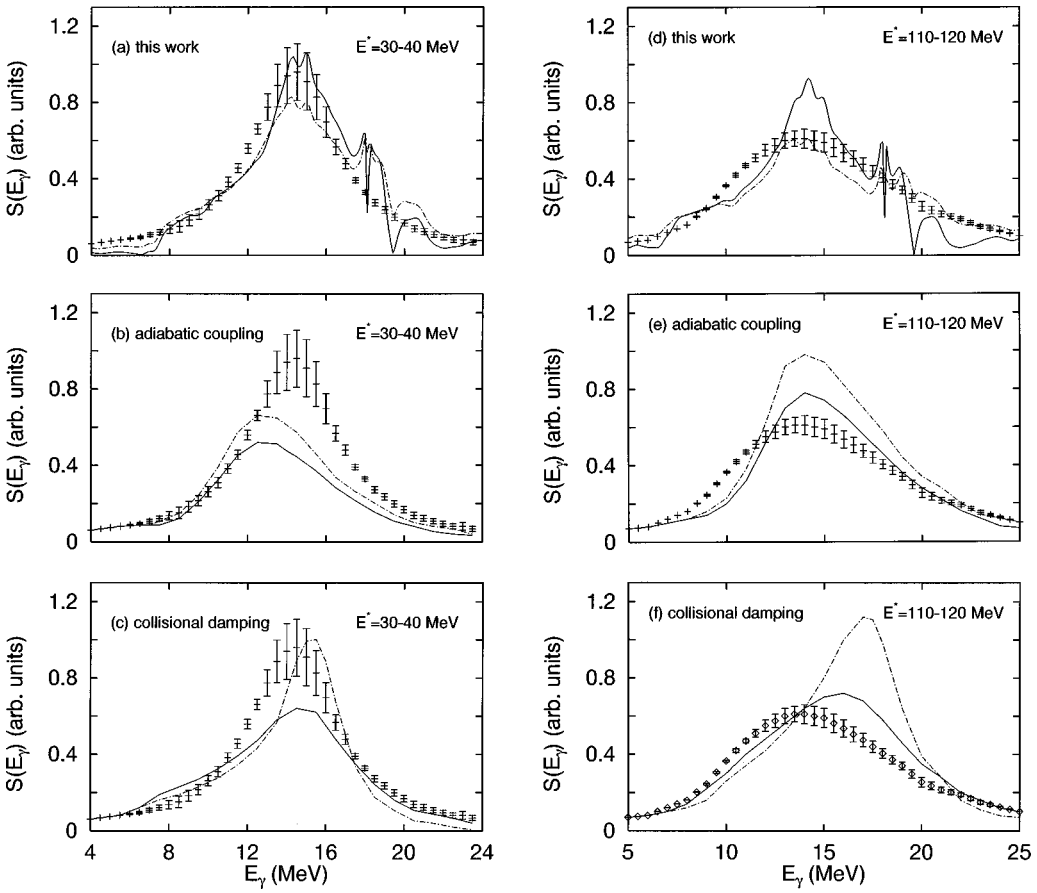

FIG. 7. GDR shapes in ^{120}Sn at (a)–(c) low 30–40 MeV and (d)–(f) high 110–120 MeV excitation energy within different models. In each panel the vertical bars denote the area of experimentally divided spectra. The results of the present work are plotted in (a) and (d), where the solid curves show the shapes calculated without the additional parameter $\Delta\gamma$, while the dash-dotted curves correspond to those obtained using $\Delta\gamma\neq 0$ (see the text). The results of the adiabatic coupling model using a strength parameter $S=1$ (dash-dotted) and 0.8 (solid) are plotted in (b) and (e). Those obtained within the collisional damping model using an in-medium (dash-dotted) and a free (solid) nucleon-nucleon scattering cross section are shown in (c) and (f).

fers a better description for the observed GDR shape in regions both of low and high excitation energies. In particular, our model gave a rather symmetric shape, which can be well approximated by a Breit-Wigner or Lorentzian curve even at high excitation energies exhausting 100% of the GDR energy-weighted sum rule (EWSR). At $E^*\sim 110$–120 MeV, which corresponds to $T\sim 3.12$ MeV [Figs. 4(d) and 4(h)], the results obtained using $\Delta\gamma=2$ MeV [Fig. 4(h)] offer better agreement with the experimental areas. The calculated strength function in the adiabatic coupling model does not follow a Lorentzian-like shape at high temperatures. Reducing the EWSR of the GDR by 20% helped the adiabatic coupling model improve the agreement with data at high excitation energies, but worsened it at low excitation energies. A similar situation takes place in the collisional damping model. Here the use of a free-space nucleon-nucleon cross section instead of an in-medium one did improve the agreement with the data at high excitation energies, but made it worse at low excitation energies.

D. Intergated yield of γ rays

The integrated yields Y_γ of γ rays in ^{120}Sn are plotted as a function of excitation energy E^* in Figs. 8(a) and 8(b). The results have been obtained upon performing the integration in Eq. (2.25) within two intervals 12 MeV $\leqslant E_\gamma \leqslant$ 20 MeV and 20 MeV $\leqslant E_\gamma \leqslant$ 35 MeV. They are compared with the data within 12–20 MeV [15,32] [Fig. 8(a)] and within (20–35) MeV [15] [Fig. 8(b)], respectively. The results reproduce reasonably well the observed saturation of the yield in both regions. A behavior similar to the case of ^{120}Sn has also been obtained in our calculations of the integrated yield of γ rays in ^{208}Pb. In this case the saturated values around 8×10^{-3} and $(10$–$12)\times 10^{-4}$ are found in the intervals 10 MeV $\leqslant E_\gamma \leqslant$ 18 MeV and 18 MeV $\leqslant E_\gamma \leqslant$ 33 MeV, respectively.

The saturation of the yield at $E^*\geqslant 300$ MeV can be interpreted here as a natural consequence of the saturation of the GDR shape and its width at $T>4$ MeV, not as a result of an exceedingly large value of the width as has been proposed previously in Refs. [28–30,32]. It is worth noticing that the value of the integrated yield in the region above the GDR (within 20–35 MeV) is more sensitive to the change of the integration limits than within the GDR region (12–20 MeV). The reason is that the integration in Eq. (2.25) involved larger energies in the region above the GDR and also that the distribution of the GDR is rather flat in the tail above 20 MeV. This may explain why sometimes the interplay between a cutoff of strength above $E^*\sim 250$ MeV and a bremsstrahlung subtraction in the experiments could describe suc-

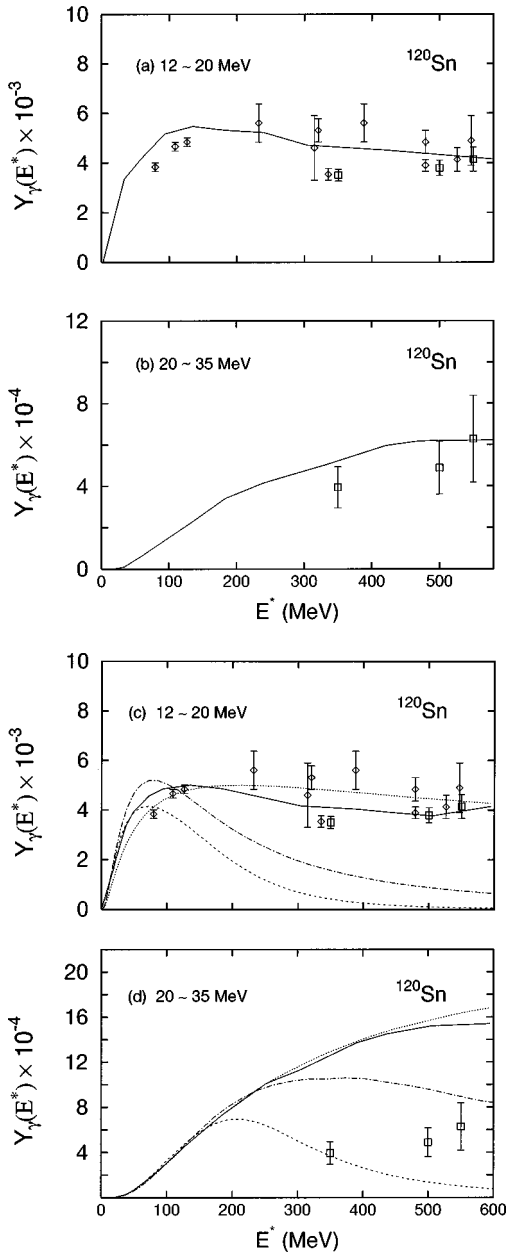

FIG. 8. Integrated yields Y_γ of the γ rays as a function of excitation energy E^* in ^{120}Sn. Squares and diamonds denote the data from Refs. [15] and [32], respectively. In (a) and (b) the solid curves denote the results of calculations in the present approach. In (c) and (d) the results of the calculations using a Breit-Wigner strength function of an ω-independent width centered at ω_{GDR} from different models are shown. Here the solid curve denotes the results obtained using the width Γ_{GDR}, the dotted curve results obtained using the width from Ref. [31], and the dash-dotted and dashed curves results obtained using the parametrizations of the Catania model in Refs. [28] and [29], respectively.

cessfully the observed γ spectra.

We would like to emphasize that the microscopic structure of the strength function $S_q^{GDR}(\omega)$ with an ω depedence of the damping $\gamma_q^{GDR}(\omega)$ is decisively important for an adequate description for both the shape and the integrated yield. As shown in Figs. 8(c) and 8(d), a Breit-Wigner distribution with a width equal to Γ_{GDR} independently of ω and centered at ω_{GDR} can describe the integrated yield only within the GDR region [Fig. 8(c)] but strongly overestimates it in the region above 20 MeV [Fig. 8(d)]. Using the FWHM from Ref. [31] leads to a similar behavior as shown by the dotted curves in Figs. 8(c) and 8(d). Meanwhile, both the parametrizations for the continuously increasing width proposed in the collisional damping model [28,29] cannot account for the data of the yields in the GDR region as well as in the region above it as shown by the dashed and dash-dotted curves.

As has been mentioned in the Introduction, the multistep CASCADE calculations using a continuously increasing width of the GDR with T yielded a saturation of the γ multiplicity in the GDR region between 12 and 20 MeV in tin isotopes, but at the expense of a strong increase of the yield above 20 MeV. In our opinion, if the observed FWHM and shape of the GDR are averaged quantities, the continuously increasing values of the width used in the CASCADE calculations of Ref. [32] may have to undergo a further appropriate averaging procedure.

IV. CONCLUSIONS

In this paper we have developed further the approach in [35] to a systematic theoretical study of the width of the GDR, its shape and the integrated yield of γ rays as a function of temperature in hot nuclei. Making use of the double-time Green's function methods, we have derived a complete set of approximated equations for Green's functions, which allow one to calculate explicitly the width of the GDR due to coupling to all the forward-going processes up to two-phonon ones in the second order of the interaction strength. The formalism has been applied to a model case, in which the GDR phonon is coupled to ph, pp, and hh through a hierarchy of higher-order graphs. The results of numerical calculations in ^{120}Sn and ^{208}Pb for temperatures increasing up to $T=6$ MeV have confirmed the prediction previously made within the simpler approximation of this formalism in [35]. The conclusions of the present paper can be summarized as follows.

(i) The total width Γ_{GDR} of the hot GDR arises mainly from the coupling of the GDR vibration to all ph, pp, and hh configurations. It increases sharply as temperature increases up to $T\sim 3$ MeV. At higher temperatures the width increase is slowed down to reach a saturated value of around 12–14 MeV in ^{120}Sn and around 10.5–11 MeV in ^{208}Pb at $T\sim 4$–6 MeV. The width increase and saturation are due to coupling to pp and hh configurations at $T\neq 0$.

(ii) The quantal width Γ_Q of the GDR due to coupling of GDR vibration to only ph configurations decreases as the temperature increases. Neglecting the two-phonon processes in the expansion to higher-order propagators results in a quantal width, which is almost independent of temperature.

(ii) The present approach describes reasonably well the experimentally extracted shape of the GDR in the recent inelastic α-scattering experiments [18] including even some details of its fine structure. As a consequence, the observed saturation of the yield of γ rays in both the GDR region and the region above it is reproduced. The fact that the present calculations show a well-defined GDR shape up to $T\sim 6$ MeV indicates the existence of the hot GDR at rather high temperatures. Hence our model has demonstrated that the hot

GDR persists as long as a nucleus exists, i.e., at least up to $T \sim 6$ MeV, in agreement with its real observation in ^{120}Sn at rather high excitation energies with a width of around 12 MeV [13–16].

Despite of the simplicity of the model under consideration it is unlikely that the main features of the results obtained within this test will be altered significantly by more sophisticated microscopic calculations except that the structure between 17 and 20 MeV will be smeared out by many complex overlaping configurations. The reason is that the hot GDR occurs in the stochastic region of high level densities and high excitation energies [44]. Even though the single-particle and collective motions, which display the regularity of the mean-field dynamics, persist in this stochastic region, all the wave functions are completely mixed to ''look the same'' so that only exact integrals of motion are kept intact [47]. As has been demonstrated in Ref. [44], equilibrium statistical averaging in this region discards all possible phase relationships between different components of wave functions so that one deals entirely with probabilities (diagonal elements of the density matrix in the energy representation or the occupation numbers considered in the present paper). Therefore, one may not need recourse to the whole set of similar individual microscopic states to obtain statistically reliable information. Surely this does not play down the more refined microscopic studies in this direction since the actual complexity of the wave functions can reveal the detail relationship between the eigenstates of the model Hamiltonian and the representation basis and therefore can shed more light on the physics of the problem. Other ingredients such as the temperature dependence of the single-particle energies, the contribution of the evaporation width at high temperatures [25], and the effects of high values of the angular momentum [26] have been also left out in the present study. While there have been some indications that these effects may not be crucial within the temperature region under consideration and/or in nuclei with mass number $A \geqslant 120$ [26,33,48], they certainly deserve thorough studies in the future.

ACKNOWLEDGMENTS

Numerical calculations were carried out by a 64-bit Alpha AXP workstation running Digital UNIX (OSF/1) at the Computer Science Laboratory of RIKEN. N.D.D. acknowledges the financial support of the Japanese Society for the Promotion of Science.

[1] K. Snover, Annu. Rev. Nucl. Part. Sci. **36**, 545 (1986); J.J. Gaardøhje, *ibid.* **42**, 483 (1992).
[2] J.L. Egido, and P. Ring, J. Phys. G **19**, 1 (1993).
[3] V.G. Soloviev, *Theory of Atomic Nuclei—Quasiparticles and Phonons* (Energoatomizdat, Moscow, 1989).
[4] G.F. Bertsch, P.F. Bortignon, and R.A. Broglia, Rev. Mod. Phys. **55**, 287 (1983).
[5] S. Drożdż *et al.*, Phys. Rep. **197**, 1 (1990).
[6] K. Takayanagi, K. Shimizu, and A. Arima, Nucl. Phys. **A447**, 205 (1988); **481**, 313 (1988).
[7] H. Sagawa, and G.F. Bertsch, Phys. Lett. **146B**, 138 (1984).
[8] N. Dinh Dang, J. Phys. G **11**, L125 (1985).
[9] P.F. Bortignon *et al.*, Nucl. Phys. **A460**, 149 (1986).
[10] N. Dinh Dang, Nucl. Phys. **A504**, 143 (1989).
[11] J.J. Gaardhøje *et al.*, Phys. Rev. Lett. **53**, 148 (1984); **56**, 1783 (1986); **59**, 1409 (1987).
[12] D.R. Chakrabarty *et al.*, Phys. Rev. C **36**, 1886 (1987).
[13] A. Bracco *et al.*, Phys. Rev. Lett. **62**, 2080 (1989); **74**, 3748 (1995).
[14] J.H. Le Faou *et al.*, Phys. Rev. Lett. **72**, 3321 (1994).
[15] P. Piattelli *et al.*, Nucl. Phys. **A599**, 63c (1996); T. Suomijärvi *et al.*, Phys. Rev. C **53**, 2258 (1996).
[16] D. Perroutsakou *et al.*, Nucl. Phys. **A600**, 131 (1996).
[17] E. Ramakrishnan *et al.*, Phys. Rev. Lett. **76**, 2025 (1996).
[18] T. Baumann *et al.*, Nucl. Phys. **A635**, 428 (1998).
[19] G. Enders *et al.*, Phys. Rev. Lett. **69**, 249 (1992).
[20] H.J. Hofmann *et al.*, Nucl. Phys. **A571**, 301 (1994).
[21] M. Gallardo *et al.*, Nucl. Phys. **A443**, 415 (1985).
[22] N. Dinh Dang, J. Phys. G **16**, 623 (1990).
[23] Y. Alhassid, B. Bush, and S. Levit, Phys. Rev. Lett. **61**, 1926 (1988); Y. Alhassid and B. Bush, Nucl. Phys. **A509**, 461 (1990); **A531**, 1 (1991); **A531**, 39 (1991); B. Bush and Y. Alhassid, Nucl. Phys. **A531**, 27 (1991).
[24] W.E. Ormand, P.F. Bortignon, and R.A. Broglia, Phys. Rev. Lett. **77**, 607 (1996); W.E. Ormand *et al.*, Nucl. Phys. **A614**, 217 (1997).
[25] Ph. Chomaz, Phys. Lett. B **347**, 1 (1995).
[26] M. Matiuzzi *et al.*, Nucl. Phys. **A612**, 262 (1997).
[27] K. Sugawara-Tanabe and K. Tanabe, Prog. Theor. Phys. **76**, 1272 (1986).
[28] P. Chomaz, M. Di Toro, and A. Smerzi, Nucl. Phys. **A563**, 509 (1993).
[29] A. Bonasera, M. Di Toro, A. Smerzi, and D.M. Brink, Nucl. Phys. **A569**, 215c (1994).
[30] V. Baran *et al.*, Nucl. Phys. **A599**, 29c (1996).
[31] R.A. Broglia, B.F. Bortignon, and A. Bracco, Prog. Part. Nucl. Phys. **28**, 517 (1992).
[32] K. Yoshida *et al.*, Phys. Lett. B **245**, 7 (1990); J. Kasagi *et al.*, Nucl. Phys. **A538**, 585c (1992); J. Kasagi and K. Yoshida, *ibid.* **A557**, 221c (1993).
[33] G. Gervais, M. Thoennessen, and W.E. Ormand, Phys. Rev. C **58**, R1377 (1998).
[34] N. Dinh Dang and A. Arima, Phys. Rev. Lett. **80**, 4145 (1998).
[35] N. Dinh Dang and A. Arima, Nucl. Phys. **A636**, 443 (1998).
[36] N. Dinh Dang and F. Sakata, Phys. Rev. C **57**, 3032 (1998).
[37] N. Dinh Dang and F. Sakata, Phys. Rev. C **55**, 2872 (1997).
[38] N. Dinh Dang, Phys. Rep. **264**, 123 (1996); in *Second European Biennal Conference on Nuclear Physics*, Megève, 1993, edited by D. Guinet (World Scientific, Singapore, 1995), p. 155; N. Dinh Dang and M. Baldo, in *Perspectives of Nuclear Physics in the Late Nineties*, Hanoi, 1994, edited by N. Dinh Dang *et al.* (World Scientific, Singapore, 1995), p. 212.
[39] P. Donati *et al.*, Phys. Lett. B **383**, 15 (1996).
[40] N.N. Bogolyubov and S. Tyablikov, Sov. Phys. Dokl. **4**, 6 (1959).

[41] D.N. Zubarev, Sov. Phys. Usp. **3**, 320 (1960).
[42] A.A. Abrikosov, A.P. Gorkov, and I.E. Dzialoshinsky, *Methods of Quantum Field Theory in Statistical Physics* (Pergamon, New York, 1963).
[43] K. Tanabe, Nucl. Phys. **A569**, 27c (1994).
[44] V. Zelevinsky *et al.*, Phys. Rep. **276**, 85 (1996).
[45] J.E. Draper *et al.*, Phys. Rev. Lett. **49**, 434 (1982).
[46] V.A. Chepurnov, Sov. J. Nucl. Phys. **6**, 955 (1967); K. Takeuchi, and P.A. Moldauer, Phys. Lett. **28B**, 384 (1969); V.G. Soloviev *et al.*, Nucl. Phys. **A228**, 376 (1977).
[47] I.C. Percival, J. Phys. B **6**, L229 (1973).
[48] M. Brack and P. Quentin, Phys. Lett. **52B**, 159 (1974); P. Bonche, S. Levit, and D. Vautherin, Nucl. Phys. **A427**, 278 (1984).